Thermodynamic study of a LiBr–H2O absorption process for solar heat storage with crystallisation of the solution

Kokouvi Edem N'tsoukpoe, Maxime Perier-Muzet, Nolwenn Le Pierrès, Lingai Luo, Denis Mangin

Energy Volume 53, 1 May 2013, Pages 179-198

Thermodynamic study of a LiBr–H2O absorption process for solar heat storage with crystallisation of the solution

Kokouvi Edem N'TSOUKPOE [a], Maxime PERIER-MUZET [a], Nolwenn LE PIERRÈS[a,*], Lingai LUO [a], Denis MANGIN [b]

[a] Laboratoire Optimisation de la Conception et Ingénierie de l'Environnement (LOCIE), CNRS UMR 5271-Université de Savoie, Polytech Annecy-Chambery, Campus Scientifique, Savoie Technolac 73376 Le Bourget-Du-Lac Cedex, France

[b] Laboratoire d'Automatique et de Génie des Procédés (LAGEP), CNRS UMR 5007-Université de Lyon 1, CPE, 69622 Villeurbanne, France

Abstract

A heat storage process by absorption is studied in this paper. It is devoted to solar domestic systems. Energy and exergy studies are performed on the ideal cycle, and prove the contribution of the solutions crystallisation to the system storage density, with an improvement of 22%. A prototype has been built and tested in conditions compatible with domestic solar thermal collectors. The process has been proved successful for heat storage. The heat charging was more efficient than the discharging phase, with respective heat transferred in the range of 1 to 2 kW and 300 to 500 W, in typical solar domestic conditions. Crystallisation has been observed, and will increase the storage density but discrepancies were found between the ideal solution and the global prototype crystallisation behaviour, possibly due to some impurities presence and a slow dissolution kinetic.

* Corresponding author. Tel.: (+33) 4 79 75 88 58; fax: (+33) 4 79 75 81 44.
E-mail addresses: nolwenn.le-pierres@univ-savoie.fr (N. Le Pierrès) ; ntsoukpoe@inkubator.leuphana.de (K. E. N'Tsoukpoe; present address : Innovation Incubator "Competence Tandem Thermal Battery", Leuphana University Lüneburg, Scharnhorststraße 1, 21335 Lüneburg, Germany), Maxime.Perier-Muzet@univ-savoie.fr (M. Perier-Muzet), lingai.luo@univ-nantes.fr (L. Luo ; present address : Laboratoire de Thermocinétique de Nantes (LTN), CNRS UMR 6607, La Chantrerie, Rue Christian PAUC, BP 50609, 44 306 Nantes Cedex 03), denis.mangin@univ-lyon1.fr (D. Mangin).
This article is based on a study first reported in the International Conference on Solar Heating and Cooling for Buildings and Industry, San Francisco, USA , 9–11 July 2012 [Conference proceedings: Energy Procedia 30 (2012) 331-341]

Energy Volume 53, 1 May 2013, Pages 179-198

Keywords: absorption; heat storage; lithium bromide/water; crystallisation.

1. Introduction: background and operation principle

Electrical batteries have given a powerful boost to the development of renewable energies, in particular solar photovoltaic and wind power plants. Similarly, long or medium term thermal batteries are expected to significantly boost the use of solar thermal energy as well as the development of waste heat recovery. Numerous studies have shown that thermochemical or sorption storages are the most suitable technologies for long-term thermal storage, because of their high energy density (about 60-800 $kWh \cdot m^{-3}$, (N'Tsoukpoe et al., 2009)) and the opportunity to achieve higher solar fraction in buildings for heating and domestic hot water production (Tanguy et al., 2012). Therefore, a lot of research efforts are currently concentrated on this type of storage process in order to push it through to the commercial stage.

Today, thermochemical or sorption applications are emerging in many different areas such as electricity fluctuation management in combination with micro combined heat and power (CHP) (Schmidt et al., 2012), e-mobility (Kerskes et al., 2012), high temperature power plants (Schaube et al., 2012), industrial applications (Lass-Seyoum et al., 2012; Shkatulov et al., 2012), vehicle thermal energy storage (Kato, 2010), heat transportation (Berthiaud et al., 2006), etc.

However, the main focus appears to be the development of a compact long-term thermal storage for buildings heating and domestic hot water production (Kerskes et al., 2012; N'Tsoukpoe et al., 2009; Tatsidjodoung et al., 2013). Most reported studies mainly focus on material characterisation or small scale tests (Lass-Seyoum et al., 2012). Only few works at medium or prototype level have been reported either with solid materials (Bales, 2008; Kerskes et al., 2012; Lass-Seyoum et al., 2012; Marias et al., 2011; Mauran et al., 2008; Michel, 2012; Zondag et al., 2010b) or with liquid aqueous solutions (Bales and Nordlander, 2005; Le Pierrès et al., 2011; Quinnell and Davidson, 2012 ; Weber, 2010). However, the introduction of this technology to the market is expected to happen in few years (by 2015 (Van Helden, 2009)), with a specific investment cost target of about 0.25 $€ \cdot kWh^{-1}$ for seasonal storage applications (Hauer, 2010; Zondag et al., 2010a).

The aim of the present work is to develop a prototype of long term solar heat storage by absorption for building heating. Solar heat is stored in summer using desorption process and released in winter via absorption (Fig. 1).

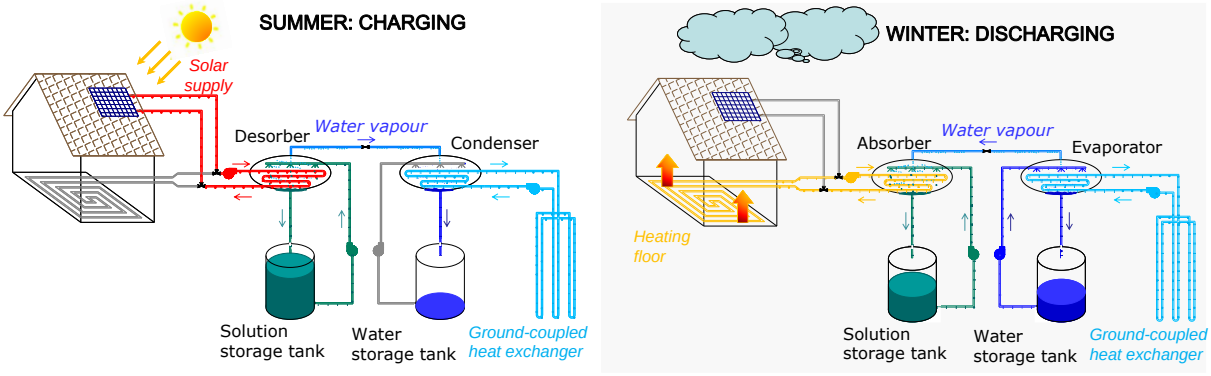

Fig. 1. Seasonal absorption storage system principle.

Four main components make up the process: a solution storage tank, a water storage tank, a generator operating alternately as a desorber or absorber, a condenser which can also operates as an evaporator. In summer or whenever solar energy is available, it is absorbed by the solar collectors and delivered to the solution that is pumped into the desorber. Then, the solution releases water vapour and increases in concentration: this is the endothermic phenomenon of desorption. The water vapour released is condensed in the condenser using a heat sink, such as a ground-coupled heat exchanger, and flows into the water storage tank. The concentrated solution leaves the desorber and flows back to the solution tank where the solution concentration increases. In heating period, in particular in winter, the evaporator is supplied with water from the water storage tank. Water vapour is then produced using a low temperature heat source such as a ground-coupled heat exchanger. This water vapour flows into the absorber where it is absorbed by the concentrated aqueous solution from the solution storage tank. The heat released by this exothermic sorption is used for heating purposes.

A multicriteria analysis on various possible absorption couples (Liu et al., 2011) led to the choice of LiBr-H_2O as the storage media for the concept feasibility demonstration. In general, when using this couple in absorption systems, the crystallisation of the solution is strictly avoided (Herold et al., 1996). However, in the case of heat storage, crystallisation can be of great interest, and has thus been subject to theoretical and experimental study. To the best knowledge of the authors of this paper, only one project dealing with the crystallisation has been identified ; the project led to a commercial product (Climatewell) that is mainly devoted to solar heating and cooling applications in the Mediterranean countries (Bales, 2008) and no detail on the crystallisation management is available.

2. Crystallisation contribution to the heat storage density and exergy analysis of the cycle

2.1. Increase of the storage density thanks to solution crystallisation

In the following, the global concentration in the storage tank is noted x and represents the ratio of the LiBr mass to the total mass (LiBr and water) in the storage tank. It thus takes into account both the liquid phase and the solid phase (LiBr dihydrate crystal in the operating conditions of the system).

The interest of solution crystallisation in the case of heat storage is presented in Fig. 2.

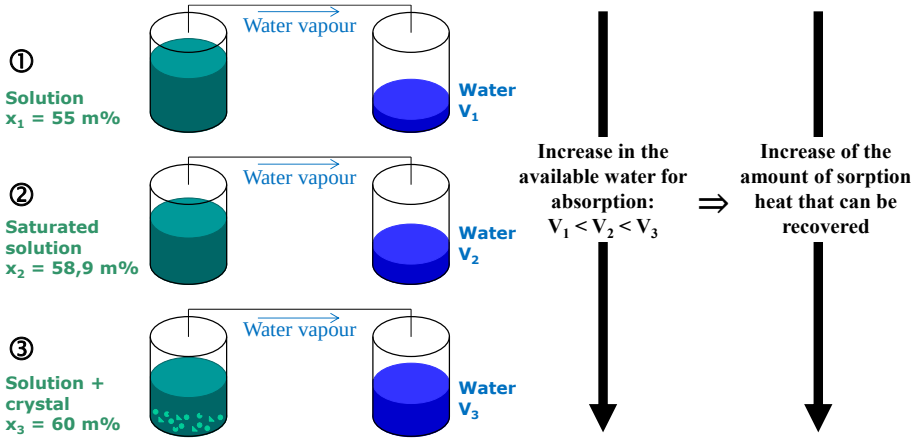

Fig. 2. Interest of the crystallisation: possible states of the system at the end of the charging phase.

In the first case in Fig.2, the final global concentration in the solution storage tank at the end of the charging period, is less than the solution solubility at the tank temperature. In the second case, the charging is stopped when the global concentration of the solution reaches the solubility. Thus, there is only liquid LiBr solution in the tank during the whole cycle for these two cases. In the third case, desorption is continued beyond the solubility line and the solution partially crystallises. The greatest mass of stored water is of course obtained in this latter case. If we now consider the following discharging period, the higher the amount of water that can be absorbed by the concentrated solution of LiBr, the greater the heat of sorption to be recovered. In the case of crystallisation in the storage tank, the absorption of water into the solution during the discharging phase leads to a progressive dissolution of the crystal into the solution. The concentration of the liquid phase in the tank thus remains constant and equal to the solubility of the solution as long as the global concentration x is higher than 58.9%. Once

all the crystal is dissolved, the global tank concentration x equals the liquid phase concentration and subsequent absorption leads to the decrease of these concentrations. As the absorption phenomena of water vapour in the solution produces more heat than the dissolution of crystals, the charging of the system towards a final global concentration higher than the solubility increases the system storage density.

Accurate data on the solubility of LiBr in water are required for accurate design and performance prediction of the process, because the theoretical storage density is very sensitive to the maximum achieved concentration (N'Tsoukpoe et al., 2012a). In addition, the solubility data inform on the stability domains of the different hydrates as a function of temperature. Unfortunately, available data in the literature on the solubility of LiBr in water (Boryta, 1970; Dean, 1999; Duvall et al., 2001; Kessis, 1965; Nývlt, 1977; Linke and Seidell, 1965) are very disparate (Fig. 3). Therefore solubility measurements in the relevant temperature range were conducted and the results are reported on Fig. 3.

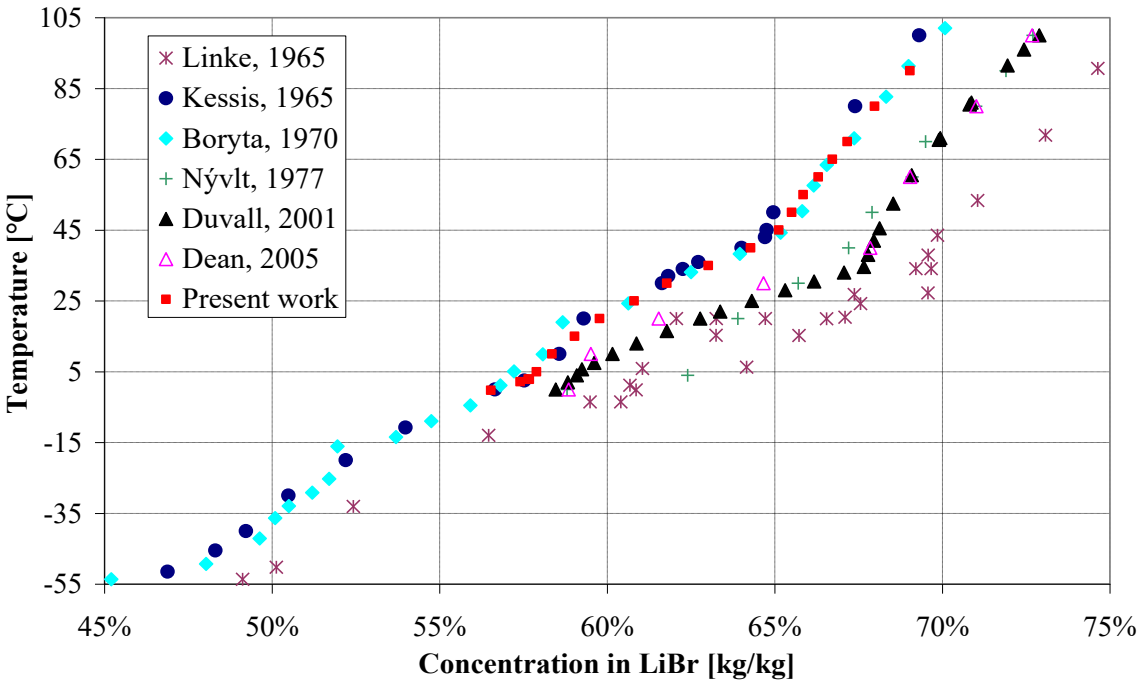

Fig. 3. LiBr solubility as a function of the temperature according to various studies.

The obtained solubility curve shows a very good agreement with that published by Boryta (1970). Above 42 °C, the monohydrate is the stable crystalline form whereas the LiBr dihydrate crystals were found stable between 3°C and 42°C. The latter observation is very important if the storage tank temperature can decrease below 3 °C. Indeed, the maximum

global concentration of the solution in the tank is then limited to 61.6 m% (LiBr anhydrous content in the trihydrate). Above this limit, only a solid block is available in the solution tank and no liquid circulation is possible for the following absorption phase. In the other case, if the tank temperature remains above 3°C, the maximum concentration of the solution could reach 70.7 m%, which would lead to a higher theoretical storage density of the system. Let us note that the presence of impurities in solution may affect somewhat theses limits and that the given concentration values cannot be reached in real systems, due to technological challenges such as the availability and circulation of the solution when necessary. However, it has been shown that crystallisation in the solution storage tank can increase the storage density by three times in given conditions and therefore, is relevant for the process competitiveness (N'Tsoukpoe et al., 2012a).

2.2. Exergy analysis of the static cycle of the process

For the exergy analysis of the process cycle, the mass conservation, the energy and exergy balances are applied to each component of the system. The solution and the water are supposed to be at the equilibrium states in all the components. The heat losses to the surroundings and the pump works are neglected. According to these hypotheses, over a whole cycle (charge+discharge), the global and LiBr mass balances for each component are respectively expressed by:

$$\sum M_i - \sum M_o = 0 \quad (1)$$

$$\sum (M.x)_i - \sum (M.x)_o = 0 \quad (2)$$

Where *M* is the global mass and and *x* is the mass fraction of LiBr in the solution.

The energy balance of each component can be written as:

$$En + \sum (M.h)_i - \sum (M.h)_o = 0 \quad (3)$$

Where *En* is the heat exchanged with the sources and *h* is the specific enthalpy.

Applying the exergy balance for a component gives:

$$Ex + \sum (M.ex)_i - \sum (M.ex)_o + Ex_d = 0 \quad (4)$$

Where *Ex* is the exergy associated to heat exchanges with the sources, *ex* is the specific exergy of the fluids and Ex_d is the exergy destroyed in the component due to the irreversibility that occurred in the process.

The exergy associated to heat exchange (*Ex*) and the specific exergy of the fluid (*ex*) are respectively calculated by:

$$Ex = En\left(1 - \frac{T_{ref}+273.15}{T+273.15}\right) \quad (5)$$

$$ex = \left(h - h_{ref}\right) - T_{ref}\left(s - s_{ref}\right) \quad (6)$$

Where s is the specific entropy of the fluid, h_{ref} et s_{ref} are the specific enthalpy and entropy of the fluid in the reference conditions of temperature (T_{ref}), pressure (P_{ref}) and composition (x_{ref}).

For the overall system, the exergy balance can be written:

$$Ex_{2,ch} - Ex_{3,ch} - Ex_{1,ch} - Ex_4 + Ex_{3,disch} - Ex_{1,disch} - Ex_{2,disch} + Ex_{d,tot} = 0 \quad (7)$$

Where $Ex_{2,ch}$ is the exergy consumed by the desorber, $Ex_{3,ch}$, $Ex_{1,ch}$, $Ex_{1,disch}$ and Ex_4 are respectively the exergy evacuated by the condenser, the solution storage during the charge and discharge phase and the water storage to the environment, $Ex_{3,disch}$ is the exergy absorbed by the evaporator from the environment, $Ex_{2,disch}$ is the exergy associated to the heat exchanged by the absorber and $Ex_{d,tot}$ is the overall exergy destroyed by the system during a whole cycle.

2.2.1 Cycle without crystallisation

The exergy evaluation of the cycle has been undergone considering the following assumptions. The desorber output concentration has to be lower or equal to the solubility of the solution at the solution storage tank temperature, to avoid crystallisation in this later. Moreover the desorber maximal temperature is 70 °C, to be compatible with solar thermal collectors operating temperatures. The absorber minimal temperature (T_{abs}) is 30 °C, to

produce heat for building heating. The condenser, the evaporator and storage tanks exchange heat with the ground (T_{gr}), considered at 15 °C (Fig 1). A temperature difference of 5 °C is assumed between the ground and evaporator and condenser in the different phases. This means that the water equilibrium temperature in the condenser (T_{cond}) is 20 °C and in the evaporator (T_{evap}) 10 °C. The operation principle is described in the introduction part of this paper. The cycles in summer and in winter described by the working fluids, considering these operating conditions, are represented in Fig. 4.

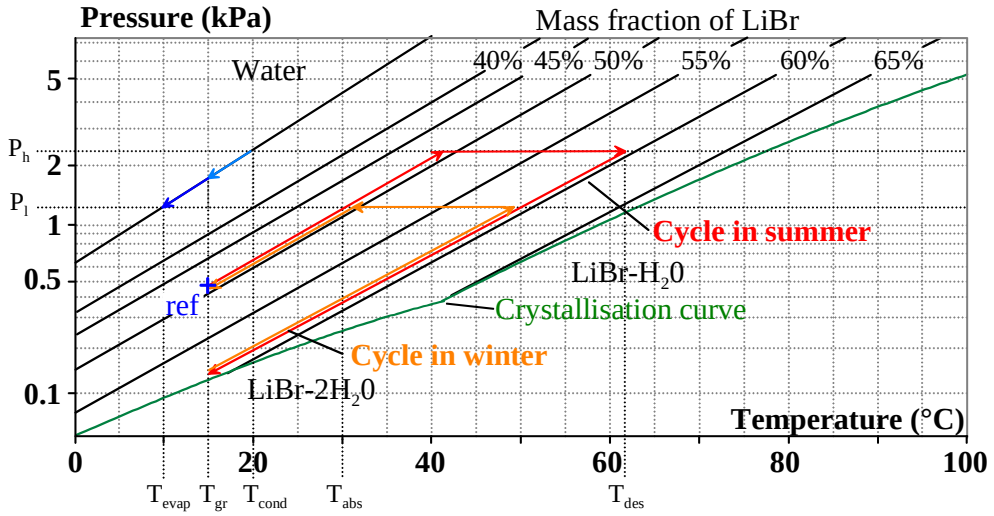

Fig 4 Operating cycles without crystallisation of the solution

The process works with a high pressure (P_h) of 2339 Pa and a low pressure (P_l) of 1228 Pa. The LiBr concentration (x) evolves between 0.49 and 0.59. The maximal temperature of the desorber (T_{des}) is 61.2 °C. The fluid properties are calculated by the correlations provided by Hellmann and Grossman (1996) for the LiBr solution properties and the correlations established by Harr et al. (1984) for water. Both are programmed in the EES software.

The reference conditions considered for this study are the temperature, pressure and composition in the solution storage tank before the desorption phase (T_{ref} = 15 °C, P_{ref} = 450 Pa and x_{ref} = 0.49).

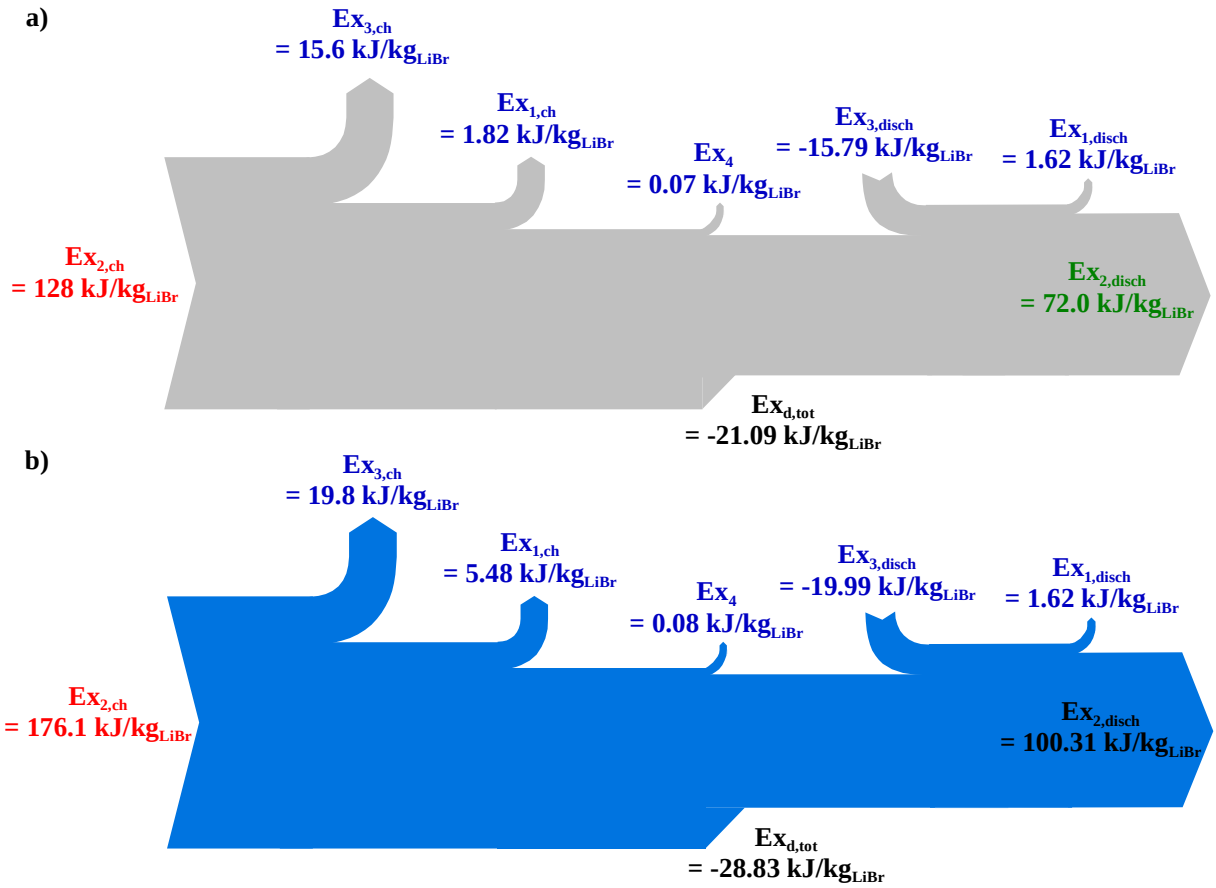

Fig. 5. Exergy exchanged between the processes and its sources a) for the cycle without crystallisation of the solution b) with crystallisation of the solution.

The exergy exchanged between the process and the sources are represented in Fig. 5a. The desorber consumed an exergy of 128 $kJ \cdot kg^{-1}_{LiBr}$ whereas the heat rejected by the absorber which is the useful effect has an associated exergy of 72 $kJ \cdot kg^{-1}_{LiBr}$. The exergy destroyed by the irreversibility that occurred in the process is 21.1 $kJ \cdot kg^{-1}_{LiBr}$.

For this static cycle, the energy efficiency defined as the ratio of the heat rejected by the absorber and the heat consumed by the desorber is equal to 0.79. The heat storage density of this system, defined as the ratio of the heat rejected by the absorber and the masse of the LiBr solution at the reference conditions is 447 $kJ.kg^{-1}_{sol}$. The exergy efficiency corresponding to the same heat transfers is 0.56. The destruction rate defined as the ratio of the exergy destroyed and the exergy consumed by the desorber is equal to 0.16.

The energetic efficiency of the system takes into account the sensible heat losses to the surroundings for a static cycle. For a real process, the share of this sensible heat would be

increased, as the solution would certainly have to be circulated several times in the desorber and absorber to achieve the desired concentrations. However, unlike the classical heat storage technologies using sensible or latent heat, the energy efficiency of the process is not dependant on the length of the phases, and it is well suited for long term storage. The exergetic efficiency is lower than the energy efficiency, as it also takes into account the temperature difference between the desorption and the absorption phases.

2.2.2 Cycle with crystallisation

To weigh the impact of crystallisation on the previous performances, the exergetic analysis of the cycle has been performed considering the followings conditions of operation. The maximal solid mass fraction in the LiBr solution storage tank at the end of the charging phase is 0.33, to keep some liquid phase available for pumping at the beginning of the following discharging phase. The crystallisation and the melting of the solid phase take place at the storage tank temperature. The temperatures of the evaporator and condenser are considered the same as the case without crystallisation.

The operating cycles considering these conditions are represented in Fig. 6. The working pressures are equal to those in the case without crystallisation. The maximal temperature of the desorber (T_{des}) is 68.9 °C and the LiBr solution concentration (x) evolves between 0.49 and 0.63.

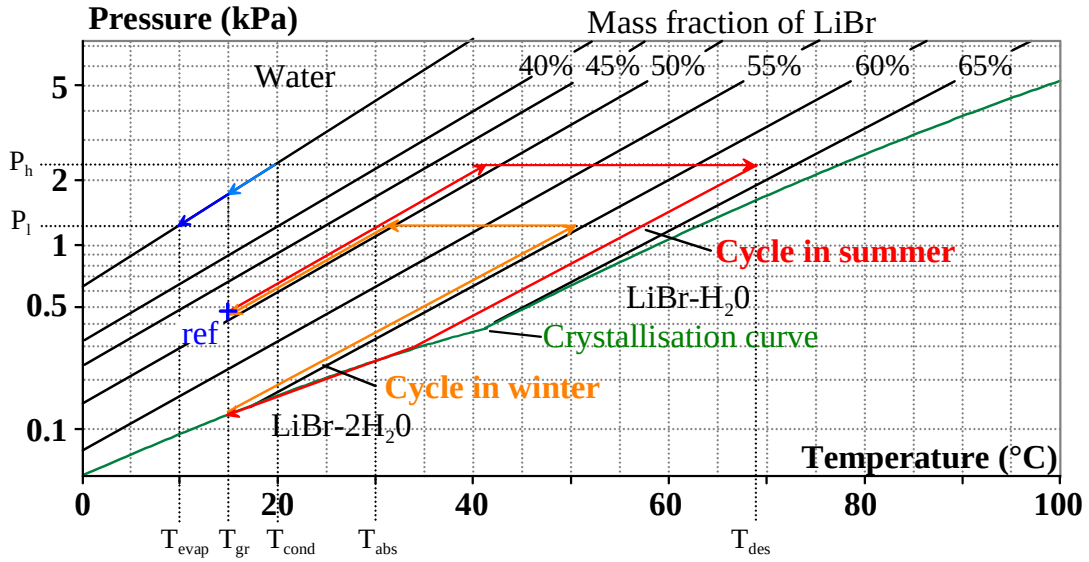

Fig. 6 Operating cycles with crystallisation of the solution

The results of the exergy evaluation for the cycle with crystallisation are summarized in Fig. 5b. In this configuration the exergy associated to the useful effect (Ex_{2a}) is equal to 100.3 $kJ \cdot kg^{-1}_{LiBr}$ and the exergy consumed by the desorber is 176.1 $kJ \cdot kg^{-1}_{LiBr}$.

In this case the energetic efficiency is equal to 0.77 and the energetic density is 546.7 $kJ.kg^{-1}_{sol}$. The exergetic efficiency is 0.57 and the destruction rate of exergy is 0.16. Crystallisation in the storage tank increases considerably the energy density of storage (+22%) without significant degradation of the system performances. The energetic efficiency is slightly lower principally because of the heat consumed to drive the dissolution of the solid in the storage tank. Because of the increased desorption temperature and despite the decrease of the energetic performances, the exergetic efficiency is slightly higher in the case with crystallisation than without crystallization. This proves the interest of enhancing the storage density of the system to over the solubility of the solution. The feasibility of this concept has thus been tested experimentally, as will be discussed in the following.

3. Prototype design

A prototype has been designed and built (Fig. 6) to demonstrate the process concept feasibility. It can store 8 kWh of heat and can provide a heat power of 1 kW to a heating floor around 30 °C.The layout of the experimental set-up is given in Fig. 7 and its main features are reported in Table 1.

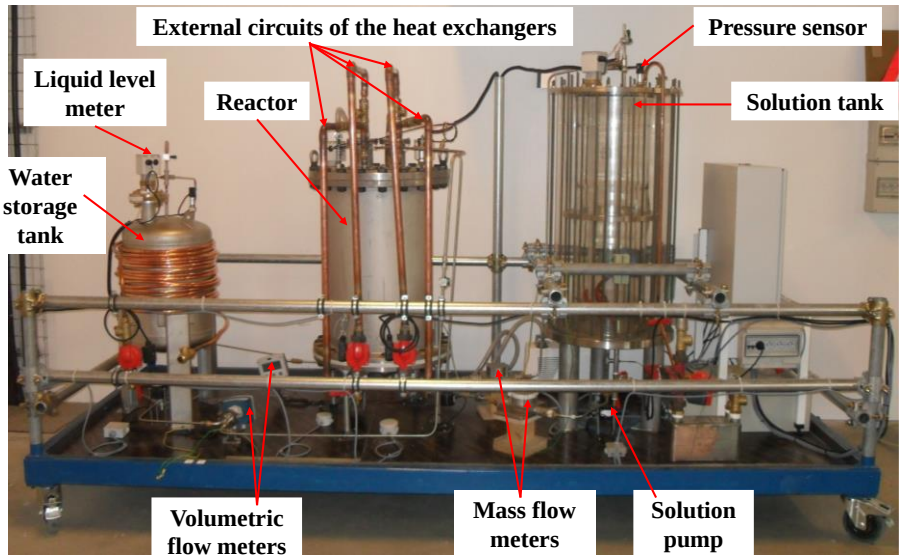

Fig. 6. Experimental set-up (before insulation).

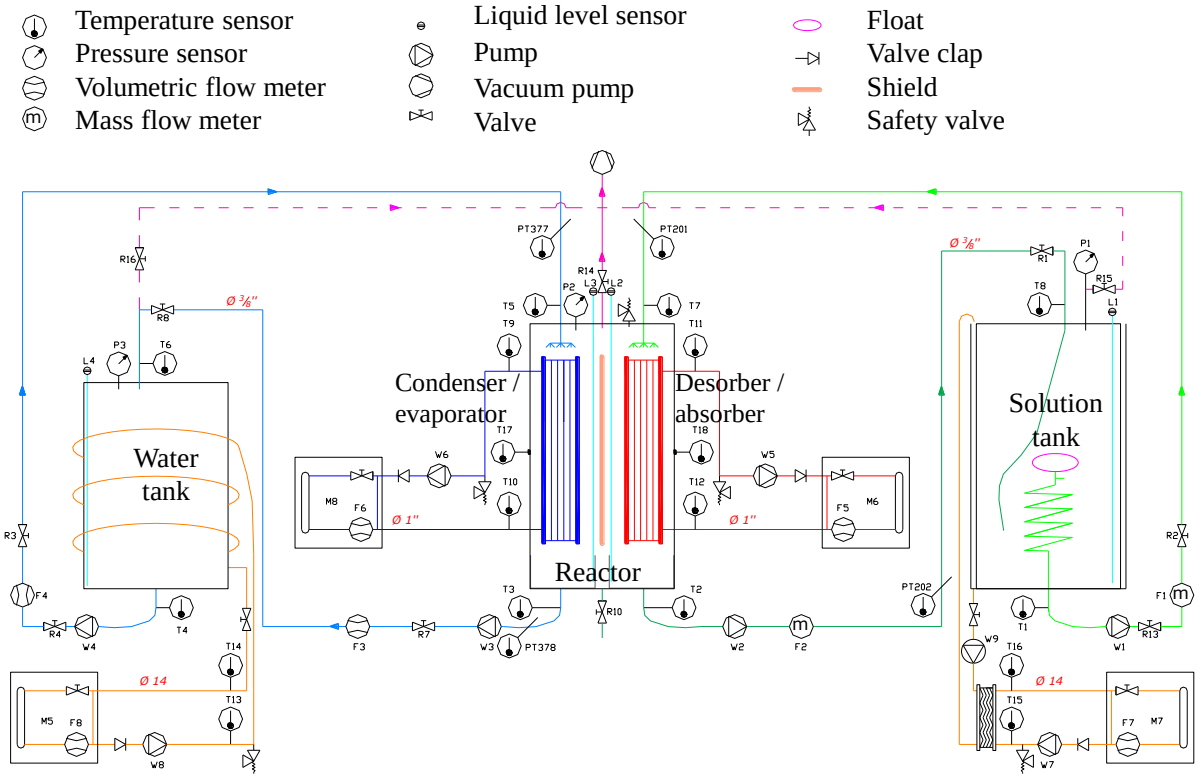

Figure 7. Layout of the experimental set-up.

Table 1. Some features of some components of the experimental set-up.

Components		Features
Reactor		
	Desorber/Absorber	Vertical falling film heat exchanger (shell-and-tubes) Total inner surface of tubes (in brass): 0.33 m²
	Condenser/Evaporator	Identical to the desorber
Solution storage tank		
	Content	46 kg of anhydrous LiBr. Initial conditions: 42.5 kg of water that is 60 l of solution (≈ 52 m%)
	Design	Glass column (inner diameter: ≈ 0.3 m) surrounded with a Plexiglas which contains a thermal bath.
Pumps (solution and absorbate)		4 magnetically coupled gear type pumps
Monitoring/Data acquisition		Computer-monitoring and control with a Labview program Data record: every 5 s

Each heat exchanger is connected to a thermal module that can provide the required heat transfer fluid (HTF) flow rate and temperature (Fig. 7). For example, the module connected to the desorber represents the solar collectors during the charging tests and the building during the discharging tests. The module that is connected to the condenser/evaporator simulates a geothermal well. Two other modules keep the storage tanks in constant surrounding temperature conditions.To ensure a sufficient solution mixing in the solution storage tank, the solution inlet in the tank (from the generator) is performed at the bottom of the tank while the solution intake (pumping toward the generator) is performed near the surface, using a floating intake. This also prevents crystal pumping when crystallisation occurs in the tank. . The prototype has been strongly instrumented, to be able to measure temperatures, pressures, mass and volume flows (and thus concentrations of the solution) and liquid levels inside the system components. The instrumentation and measurement precision with the corresponding uncertainty analysis are detailed in Appendix B. A more detailed description of the prototype is given in (N'Tsoukpoe et al., 2013).

4. Experimental tests of the prototype

The prototype has been tested in static and dynamic operating conditions that are compatible with solar domestic systems. More than forty tests have been conducted for charging and discharging phases. A charging and a discharging test during which crystals are present in the solution storage tank are presented and analysed below.

4.1. Charging test

4.1.1 Crystallisation matters

Fig. 4 shows the observed temperatures during a static charging test in which the solution flow rate at the desorber inlet was 22 $l \cdot h^{-1}$. The HTF flow rates in the desorber and the condenser were 720 and 360 $kg \cdot h^{-1}$, respectively.

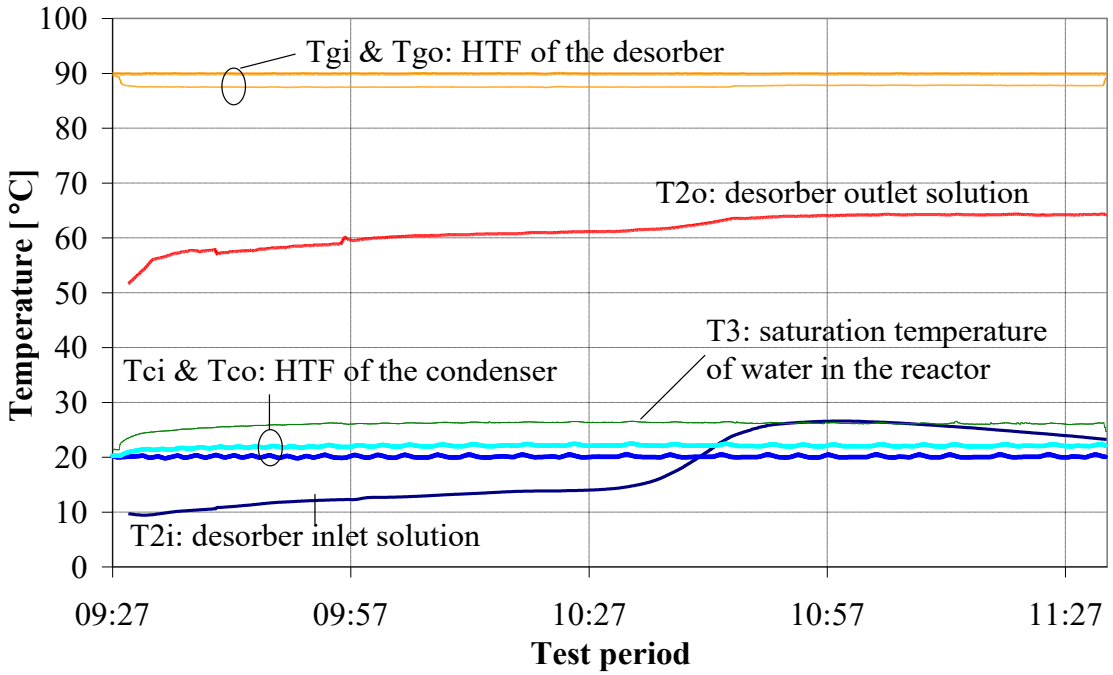

Fig. 4. Temperatures during a charging test (16/09/2011).

The observed desorption temperature was around 60 °C (T_{2o} in Fig. 4) for a condensation temperature of about 25 °C (T_{ci} and T_{co}). These temperatures remain quite constant during the two-hour test.

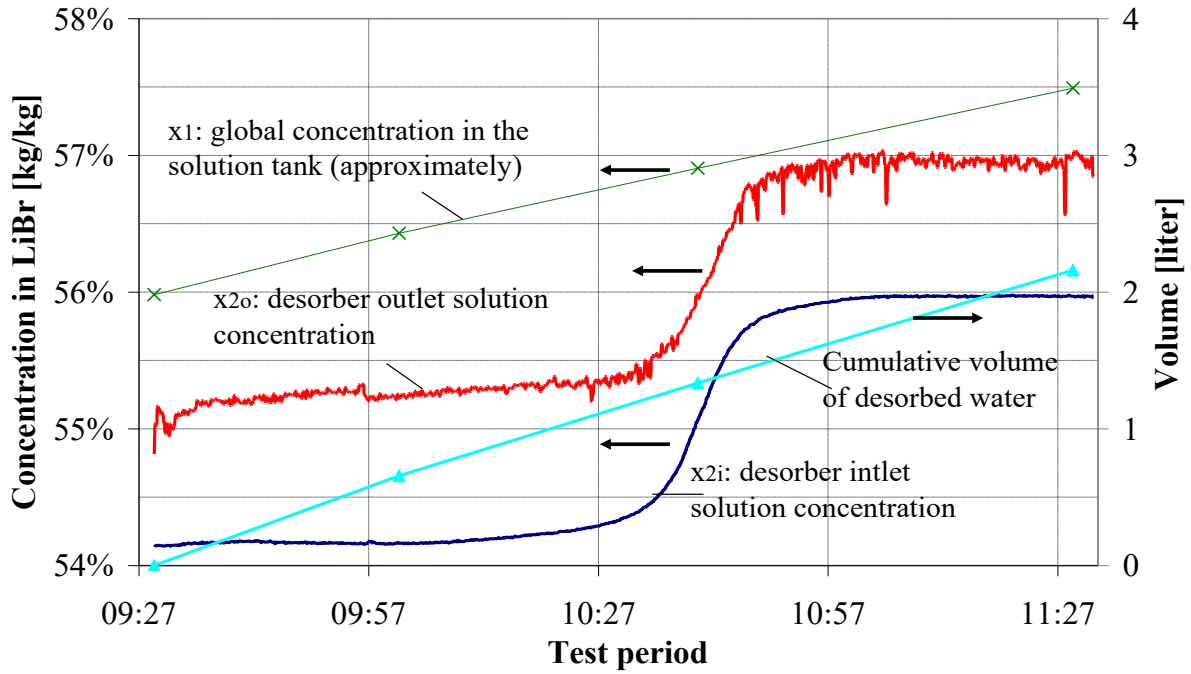

Fig. 5. Concentration and mass of desorbed water evolution during a charging test (14/09/2011).

The concentrations of the solution at the inlet and outlet of the desorber are shown on Fig. 5. The total mass of desorbed water during this two-hour test is about 2.2 kg. The change of the concentration of the solution in the desorber is relatively low (about 1 m%), compared to conventional absorption machines (5 m% approximately, (Florides et al., 2003; Herold et al., 1996)). Improved mass transfer is then desirable. The concentration of the solution leaving the solution tank is lower than the total concentration of the solution in the tank, which means that the solution in the tank is not homogeneous (in concentration) during the charging tests. The solution tank behaves as a plug flow reactor during the charging tests (N'Tsoukpoe et al., 2013). The global concentration in the tank at the end of the reported test (about 57.5 m%, Fig.6) is lower than the solubility concentration (> 58 m% at the tank temperature). However, crystals were observed in the tank and may be due to concentration stratification in this component. This stratification in concentration is also suggested by direct observations of the storage tank (Fig. 6).

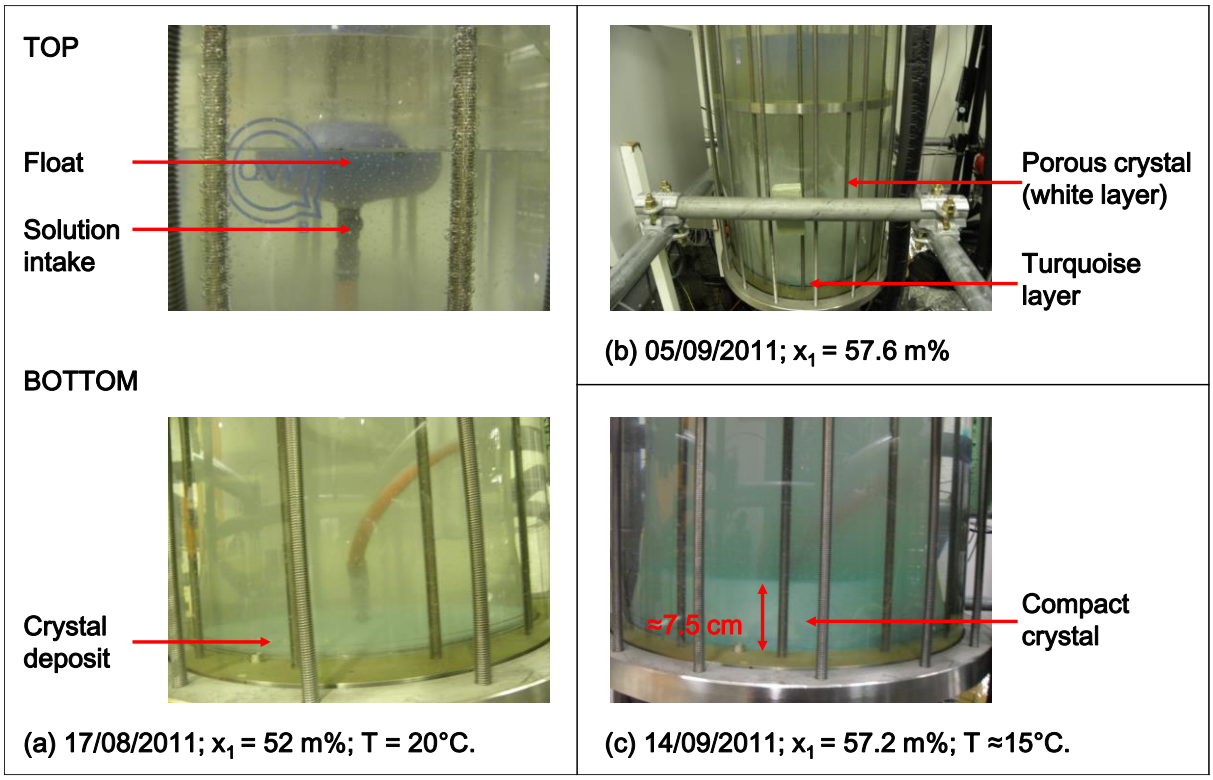

Fig. 6. Crystallisation in the solution storage tank.

Indeed, two weeks after the introduction of the solution in the storage tank (03/08/2011), deposits can be seen at the bottom of the solution tank (Fig. 6a), which is cloudy while the top is clear (no desorption or absorption has been conducted in the meantime; only hydraulic verifications have been performed). Further analysis of the storage tank outlet solution concentration lead in the same direction (N'Tsoukpoe et al., 2013): the tank outlet concentration as a function of the global concentration in the tank (values at the start of the tests) presents a linear trend with a gap of 2 m% (the tank outlet concentration is in general about 2 m% below the global concentration in the tank).

In further tests involving crystallisation in the storage tank, the amount of crystal is far greater than that expected considering the overall concentration of the solution and its temperature (between 10 °C and 20 °C). The first crystals observed are very porous (Fig. 6b) and the residual liquid is trapped in, leaving only a small quantity of liquid available for pumping. However, these crystals take part to the absorption process, and are dissolved during the following discharging phases, thus increasing the heat storage capacity of the system. Later, a part of the crystal block becomes compact (turquoise solid layer at the bottom of the tank in Fig. 6c) and stays undissolved until the end of the test campaign. This phenomenon needs further investigation. It can be explained by a progressive increase of the compactness of the crystal due to the length of the storage phase. In this case, the decrease of

the porosity of the crystal hinders its following dissolution by the solution. Another explanation is the formation of other chemicals in this slab, as is suggested by its turquoise colour. Indeed, a part of the heat exchanger was made in brass aluminium (CuZn22Al2), a copper alloy renowned for its resistance to corrosion, but which could have been attacked by the LiBr solution.

Contrary to the pure crystal of LiBr, which is white and translucent (Fig. 9b), this remaining part is turquoise (Fig. 9c), like some first precipitations that have been identified in the solution tank (Fig. 9b). Now, considering the fact that the tubes of the falling film heat exchanger are made of brass (an alloy consisting of copper and zinc and particularly renowned for its corrosion resistance) and no corrosion inhibitor was intended to be used in the first series of tests, it is estimated that this turquoise blue layer contains copper corrosion products from the desorber. The turquoise layer could therefore be a mixture of CuBr or CuBr and LiBr hydrates. Indeed, the products resulting from the corrosion of copper in LiBr aqueous solution are a mixing of copper bromide (CuBr) and some copper oxydes and hydroxydes ($CuO{\cdot}Cu[OH]_2$, $CuBr_2{\cdot}3Cu[OH]_2$) (Muñoz-Portero et al., 2006). The CuBr is greenish-grey, crystalline, insoluble in water (Berthemot, 1830a) and indecomposable by heat in the absence of air (Berthemot, 1830b). The concentrated solution is greenish while a dilute solution is blue (Jones et al., 1910). This description of the CuBr corresponds to our observation. Furthermore, the above mentioned copper components are not soluble in water (Muñoz-Portero et al., 2006). Therefore, they may have been favourable nucleation sites for crystallisation and have shifted the equilibrium solubility of LiBr.

The repeated breaking of the vacuum for some interventions, and thus the entrance of oxygen, has probably favoured the corrosion of the alloy tubes. In turn, the corrosion could have impacted negatively the performance of the desorber/absorber.

4.1.2 Energy analysis of a charging phase

The powers exchanged in the desorber and the condenser during the presented charging phase are shown in Fig. 7. Uncertainty analysis of these results is presented in Appendix A2. The power actually received by the solution in the desorption process Q_2' is also displayed. These powers are calculated as follow:

$$Q_2 = m_g \cdot Cp_g \cdot \left(T_{gi} - T_{go}\right) \quad (8)$$

$$Q_3 = m_c \cdot Cp_c \cdot (T_{ci} - T_{co}) \quad (9)$$

$$Q_2' = m_{2o} \cdot h_{2o} + m_{vap} \cdot h_{vap} - m_{2i} \cdot h_{2i} \quad (10)$$

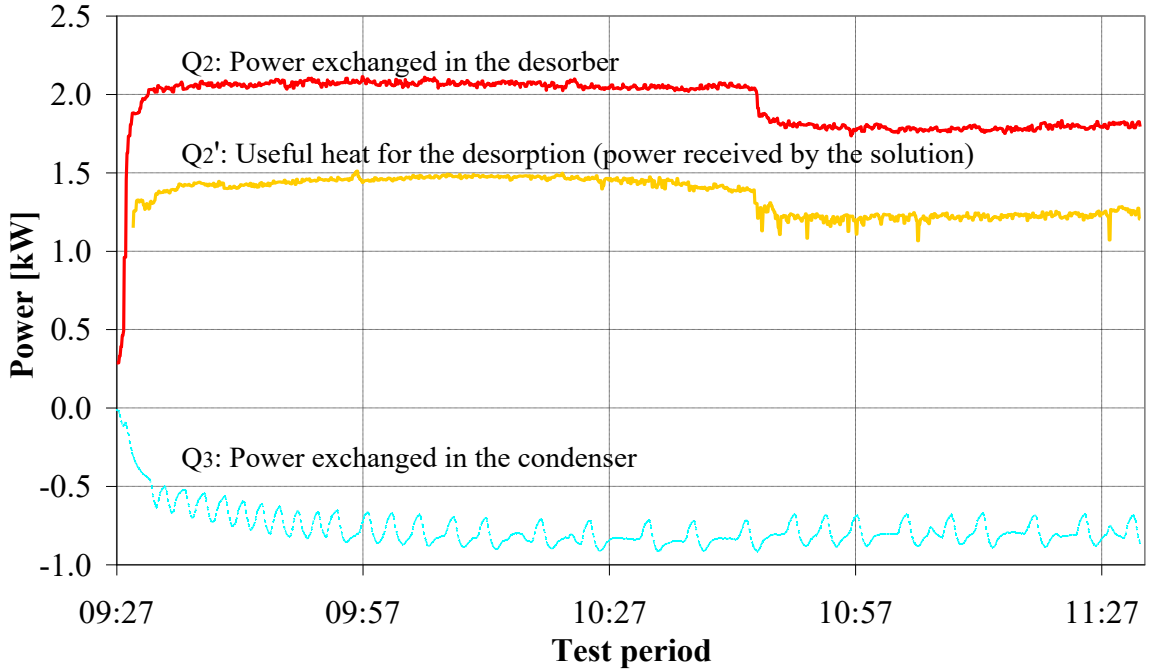

Fig. 7. Powers exchanged during the charging test.

Q_2' corresponds to the sum of the heat required for water desorption and the sensible heat transferred to the solution. h_{vap} is the enthalpy of the superheated water vapour at the measured desorber outlet solution temperature T_{2o} and the measured pressure P_2 in the reactor. The mass of the released water vapour m_{vap} is calculated as the difference between the desorber inlet (m_{2i}) and outlet (m_{2o}) solution flow rates. Due to some solution accumulations in a collector under the desorber, the measured flow rate m_{2o} is not always the actual desorber outlet flow rate. So, m_{2o} is evaluated based on the salt mass conservation balance (Eq. (11)):

$$m_{2i} \cdot x_{2i} = m_{2o} \cdot x_{2o} \quad (11)$$

The previous procedure is acceptable, since the desorber oulet solution enthalpy changes very slightly: a maximal error of 3% on the value of the enthalpy for a change in the concentration of 1 m% at 60 °C.

Q_2' shows the same trend as the power exchanged in the desorber Q_2, with a constant difference of about 0.5 kW (Fig. 7). This difference corresponds to the heat loss to the ambient.

The energy balance is then performed on the desorber for the whole test by comparing the useful energy for the desorption process En_2' (integral of Q_2' over the time) to the total energy

provided through the HTF to the desorber En_2 (integral of Q_2 over the time, Fig. 8). The difference between En_2 (4 kWh) and En_2' (2.8 kWh) is very high (1.2 kWh). This heat loss corresponds to about 30% of the total energy supplied to the desorber En_2. A better conception and insulation of the prototype is then required.

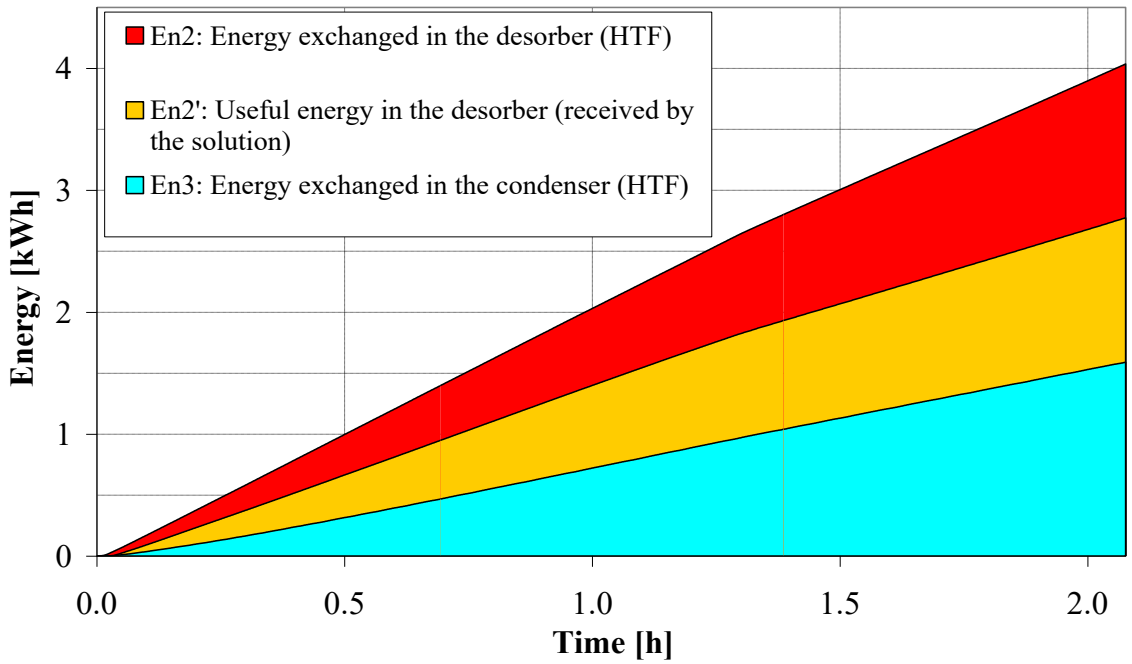

Fig. 8. Energies exchanged in the desorber and condenser during the charging test.

Another comparison is made between the useful desorption energy En_2' and the heat rejected by the condenser En_3 (integral of Q_3 over the time). The heat removed in the condenser En_3 (1.6 kWh) represents 57% of the desorption heat En_2' (2.8 kWh). The value is consistent with a theoretical analysis presented in (N'Tsoukpoe et al., 2012a): the condensation heat is about 60% of the desorption heat for a classical absorption chiller (with the desorber inlet solution at 30 °C at least) and about 50% for a storage process with a desorber inlet solution temperature of 5 °C; here the desorber inlet solution temperature is between these values (mean temperature of 18°C; Fig. 4). The recovery of the heat removed at the condenser may improve the thermal efficiency of the process. For instance, this heat can be partially used to preheat the desorber inlet solution.

4.2. Discharging test

Fig. 10 and Fig. 10 show the observed concentrations and temperatures during a static discharging test in which the solution flow rate at the absorber inlet was 43.5 $l \cdot h^{-1}$. The HTF flow rates in the absorber and the evaporator were set to 360 $kg \cdot h^{-1}$.

The mass of absorbed water is 1.5 kg during this three-hour test. The concentration of the solution feeding the absorber decreases gradually with an almost constant slope (Fig. 9), unlike in the charging tests. The change in concentration of the solution between the inlet and outlet of the absorber also remains practically constant (approximately 1 m%). This means that the mass transfer in the absorber (flow rate of absorbed water vapour) is roughly constant during the test.

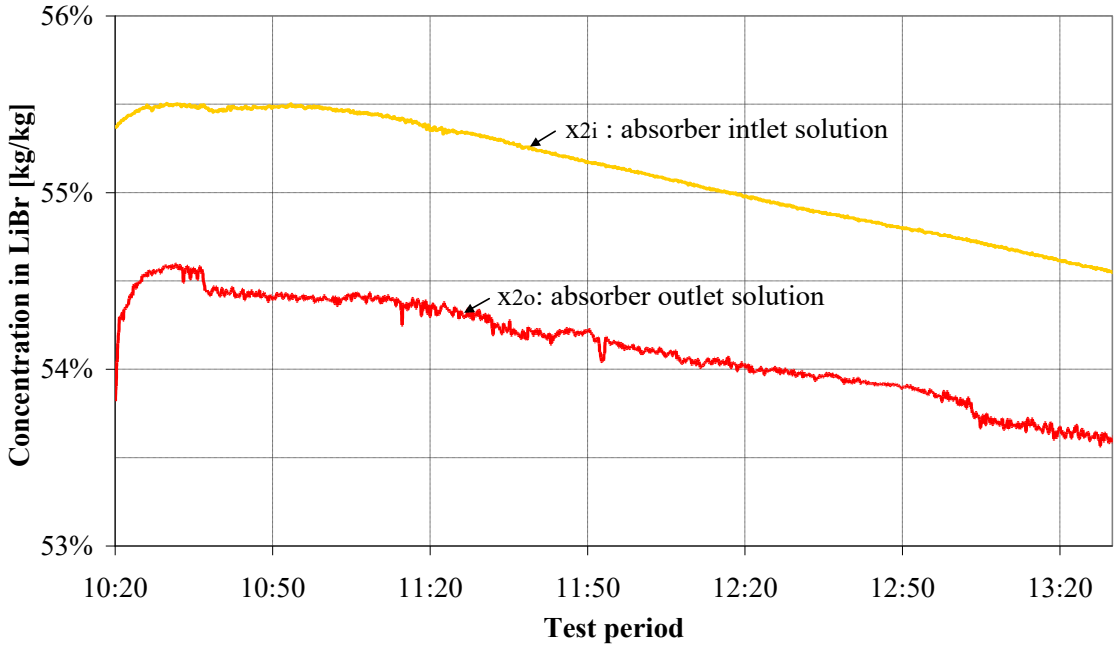

Fig. 9. Concentrations evolution during the selected discharging test (14/09/2011)

For all the discharging tests performed, the change of the solution concentration along the absorber is relatively small (1 to 1.5 m%), as in the desorption tests. Now, the change of the solution concentration is a key performance indicator for absorbers (Hihara and Saito, 1993) especially for low-capacity absorption machines (Fujita, 1993). Indeed, a large concentration change means a large heat release in the absorber and less circulation loss (N'Tsoukpoe et al., 2012a).

The solution enters the absorber at 15-20 °C and leaves it at a mean temperature of 31 °C (Fig. 10). However, the HTF enters the absorber and leaves it at practically the same temperature (26 °C). The reasons of the low performance of the absorber are already discussed in (N'Tsoukpoe et al., 2013).

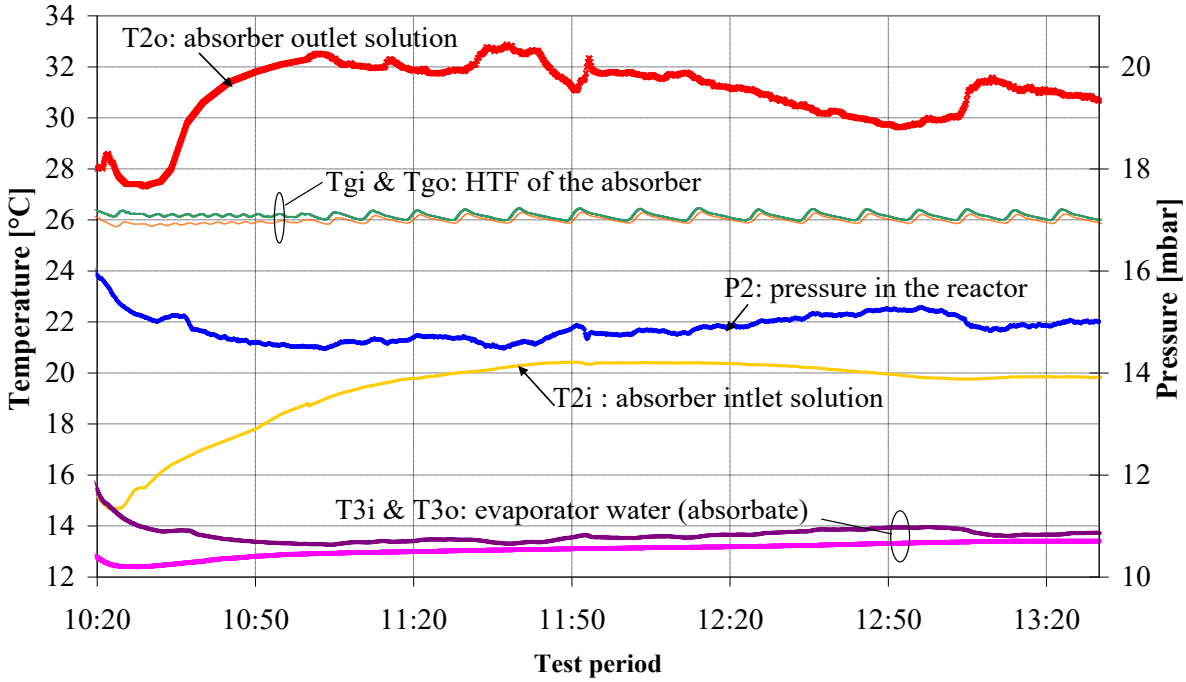

Fig. 10. Temperatures during the discharging test (14/09/2011).

Since the power exchanged between the solution and the HTF is very small as well as the temperature change of the HTF in the absorber, the uncertainty of the evaluation of the heat absorbed by the HTF is to high to be discussed. Thus, to evaluate the absorbtion heat produced, we calculate the sensible heat gained by the solution as it passes through the absorber, following Eq. (12). This calculation actually underestimates the real heat produced in this component, as it disregards the heat loss to the ambient and the heat transferred to the HTF. It is also assumed that the solution mass flow rate change is negligible (it is actually less than 2%):

$$Q_{2min} = m_{2i} \cdot (h_{2i} - h_{2o}) \qquad (12)$$

In Eq. (12), the temperatures and the concentrations of the solution at the absorber outlet and inlet are measured, so Q_{2min} can be calculated with an acceptable uncertainty (see Appendix A2). The power exchanged in the evaporator by the HTF (Eq. (9)) is also calculated and the obtained values are displayed on Fig. 11.

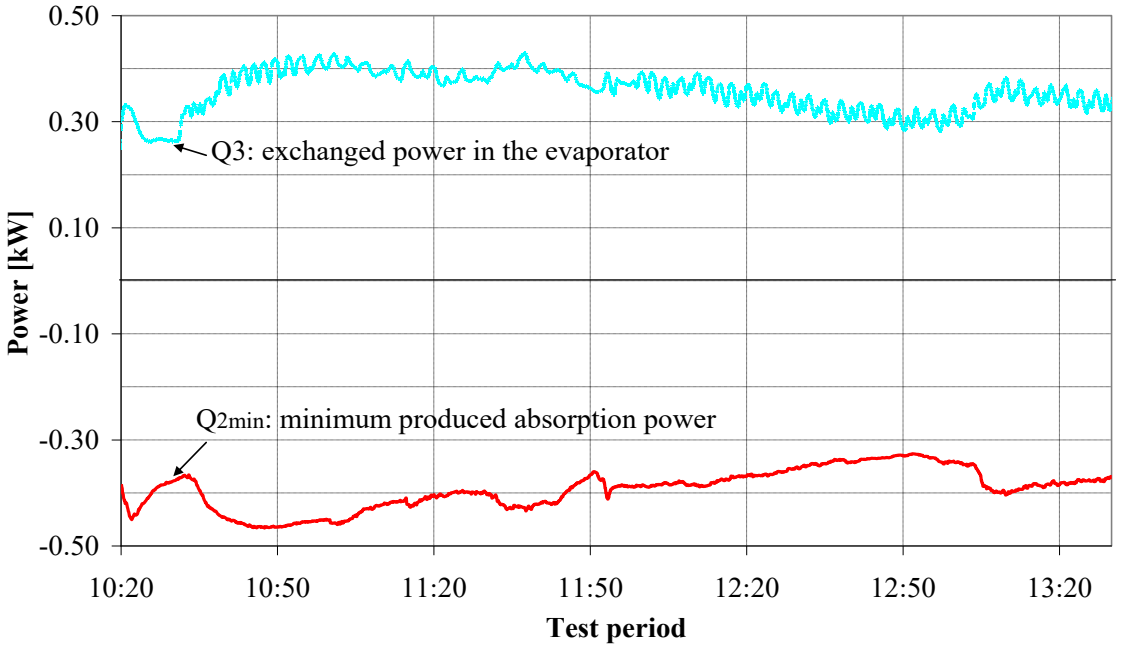

Fig. 11. Minimum produced absorption power and power exchanged in the evaporator.

Both depicted powers show the same trend over the time. The minimum absorption power is small (mean value = 0.4 kW) compared to the design target (1 kW). However, if the heat exchange with the HTF were effective (heat removal), the produced power would be higher because in the same inlet conditions, more refrigerant is absorbed in a cooled (non isothermal) absorber than in an adiabatic one (Ventas et al., 2010). Then, the heat transfer, rather than the mass transfer, seems to be the main limiting phenomenon.

During all this 3-hour test, crystals were present in the solution tank. The solution circulation in the tank did not seem to contribute substantially to the dissolution of the crystal block, at least from visual estimation. An explanation could be that the dissolution kinetic is low for such a low concentration fluctuation around the solubility limit. However, apart from the compact turquoise slab at the bottom of the tank (fig 7.c), the porous crystal layer could be dissolved and re-produced during the series of tests performed.

6. Conclusion and outlooks

Absorption solar heat storage is a promising option, especially when crystallisation of the solution is allowed in the storage tank. Energy and exergy analysis show the interest of the increase of the solution concentration at the end of the charging phase, with an efficiency of the process quite unchanged, and a large increase of the storage density of 22%, with only

33m% of solid in the tank. A prototype has been built and tested under conditions compatible with a domestic solar power plant: the thermal storage has been proven. The absorption and desorption phases have been analysed. They show that the desorber should be improved, to enhance the heat transfer with the heat transfer fluid and decrease the heat losses to the surroundings. The change of the concentration of the solution in the desorber and absorber is about 1 m% during all the tests. The crystals formations and dissolutions have been observed. The charging and discharging phases with crystals in the tank have been possible. The crystallisation behaviour, however, is still subject to discussion: the ideal solution solubility differs from observations made on the global prototype and the dissolution kinetics seem to be slower than expected. This is certainly due to differences in the purity of the solution, because the presence of solid impurities in the solution fastens the crystallisation of the LiBr, and could even shift the position of the solubility curve. Moreover, the corrosion of the metal components of the global system can produce new chemical compounds that accumulate in the solid form in the solution tank and are difficult to dissolve during the discharging phases. This issue still has to be looked at in detail, as the system would have to be reliable over several decades in domestic systems. Moreover, LiBr-H_2O is a possible candidate for the working pair, and has been used in this study for the feasibility demonstration of the concept but its cost is too high to be used in actual seasonal solar heat storage systems. Thus, other pairs will have to be studied and characterised for this application, with special emphasis on crystallisation.

Acknowledgements

We thank the ANR (French National Research Agency) for its financial support under the research projects PROSSIS ANR-07-Stock-E-08, ESSI ANR-08-Stock-E-04 and PROSSIS2 ANR-11-SEED-0011-01. The authors are grateful to their project partners from CEA (C. Paulus, G. Tanguy) for their organisation support, and T. Goldin, F. Bruyat and L. Degeronimi for their technical support.

Nomenclature

General

Cp	specific heat [$J \cdot kg^{-1} \cdot °C^{-1}$]

En	energy [J·kg_{LiBr}^{-1}]
Ex	exergy [J·kg_{LiBr}^{-1}]
ex	specific exergy [J·kg^{-1}]
h	specific enthalpy [J·kg^{-1}]
HTF	heat transfer fluid
m	mass flow rate [kg·s^{-1}]
m%	mass percent
M	mass [kg]
P	pressure [Pa]
Q	heat [W]
s	specific entropy [J kg-1 K]
T	temperature [°C]
x	mass fraction of lithium bromide in the solution [m%]

Subscripts/Superscripts

1	solution storage
2	desorber or absorber
3	condenser or evaporator
4	water storage
c	condenser/evaporator heat transfer fluid
abs	absorption
cond	condensation
ch	Charging (desorption) phase
disch	Discharging (absorption) phase
d	destruction
des	desorption
eq	equilibrium conditions
evap	evaporation
g	desorber/absorber heat transfer fluid
gr	ground
i	inlet
min	minimum
o	outlet
ref	reference
sol	Solution
tot	total

Greek symbols

ρ	density [kg·m^{-3}]

Appendix A. The measuring instruments and their uncertainties.

Table A.1. The measuring instruments and their uncertainties.

Variable	Measuring instruments	
	Reference and provider	Main characteristics
Storage tanks inlet and outlet temperature (T_{1i}, T_{1o}, T_{4i}, T_{4o})	Resistance Temperature Detector sensor Class B (IEC 60751) TC Direct	Range: -50 °C to + 200 °C Uncertainty: $\Delta T = 0.3 \pm 0.005\theta$ θ = absolute value of the measured temperature
HTF temperature (T_{gi}, T_{go}, T_{ci}, T_{co})	Calibrated RTD sensor CEA-INES	Uncertainty: ΔT: ± 0.2 °C
Vapour pressure (in the reactor and storage tanks)	Pressure transducer SEN-32320212010521 Kobold	Range: 0-2500 Pa (abs.) Uncertainty: ΔP: ± 25 Pa
Liquid level (in the storage tanks and collectors in the reactor)	Capacitive level meter NMC S1 9G9 03 L_1[a]: 980 mm $L_2 = L_3$: 791 mm L_4: 733 mm Kobold	Uncertainty: Δl: ± 2 mm
Mass flow rate (m_{2i}, m_{2o}), density and temperature of the solution (T_{2i}, T_{2o})	Coriolis mass flow and density meter RCCS31-A41G9SH/K4 Yokogawa	Flow rate uncertainty: $\Delta m/m < 0.05\%$ Density uncertainty: $\Delta\rho$: ± 1 kg·m^{-3} Temperature uncertainty: $\Delta T < 0.2$ °C
Water flow rate (absorbate)	Turbine flowmeter PEL-L005 S10 K Kobold	Uncertainty: Δv: ± 1 l·h^{-1}
HTF mass flow rate (m_g, m_c)	Coriolis mass flow and density meter Micro Motion F050S	Uncertainty: ± 0.1%

[a] Length of the liquid level transmitter. L_1 corresponds to the solution tank.

Appendix B. Uncertainty analysis

The references for the properties of Water and LiBr aqueous solution properties used in the analysis are given as follows:

Properties of water saturated and superheated of water vapour: Saul and Wagner, 1987; Hellmann and Grossman, 1996.

Density of LiBr solution : Lee et al., 1990.

Thermodynamic properties of lithium bromide of LiBr solution: Hellmann and Grossman, 1996.

The analysis is performed based on the error propagation theory as described by Moffat (1988) and Figliola (2010). The results are summarised in Table B.1 and the calculation steps are detailed below.

Table B.1. Uncertainty estimation of the calculated parameters.

Parameter		Uncertainty
Power (HTF side)	Q_3	$\Delta Q = 0.1\ kW$ for tests with m_g = 360 kg·h^{-1}
	Q_2	$\Delta Q = 0.2\ kW$ for tests with m_g = 720 kg·h^{-1}
Power (solution side, desorption)	Q_2'	$\frac{\Delta Q_2'}{Q_2'} = 12\%$
Power (solution side, absorption)	Q_{2min}'	$\frac{\Delta Q_{2min}'}{Q_{2min}'} = 7\%$
Solution concentration at the desorber/ absorber inlet and outlet	x	$\Delta x \approx 0.2$ m% $\Delta x/x = 0.4$ %
Mass of desorbed or absorbed water	M_4	$\Delta M_4 = 0.4$ kg

B1. Solution concentration

The solution concentration at the desorber/absorber inlet (x_{2i}) and outlet (x_{2o}) is calculated based on the density and temperature measurements by Coriolis flowmeters (Table A.1), using a correlation suggested by Lee et al. (1990).

The density is a monotonically increasing function in the range involved in the tests; the solution concentration can then be expressed as follows:

$$x = \frac{\left(K_1 \cdot T + K_2\right) + \sqrt{\left(K_1 \cdot T + K_2\right)^2 + K_3 \cdot T + K_4 \cdot \rho + K_5}}{K_6} \qquad \text{(B.1)}$$

K_1 = 0.571749 K_4 = 5499.16

K_2 = -314.66676065 K_5 = - 5797729.75456528

K_3 = 1833.38144988 K_6 = 2749.58

Since the temperature and the density are measured by the same instrument, their errors are correlated. As the differential of Eq. (A.5) would appear to be somewhat complex, a sequential perturbation approach (Moffat, 1988; Figliola et al., 2011) is used to estimate the uncertainty.

Fig. B.1 shows the relative uncertainty of the solution concentration, with the temperature difference and the density uncertainties of 0.2 °C and 1 kg·m^{-3}, respectively. The density value is perturbed sequentially twice in order to take into account the average absolute deviation of the correlation of Lee et al. (1990).

The temperature uncertainty has no significant effect on the overall uncertainty. The relative uncertainty of the solution concentration can be considered less than 0.5% (Fig. B.1a; the considered density and temperature ranges includes the range that is presented in this work). That results in an absolute uncertainty of about 0.2 m% (Fig. B.1b).

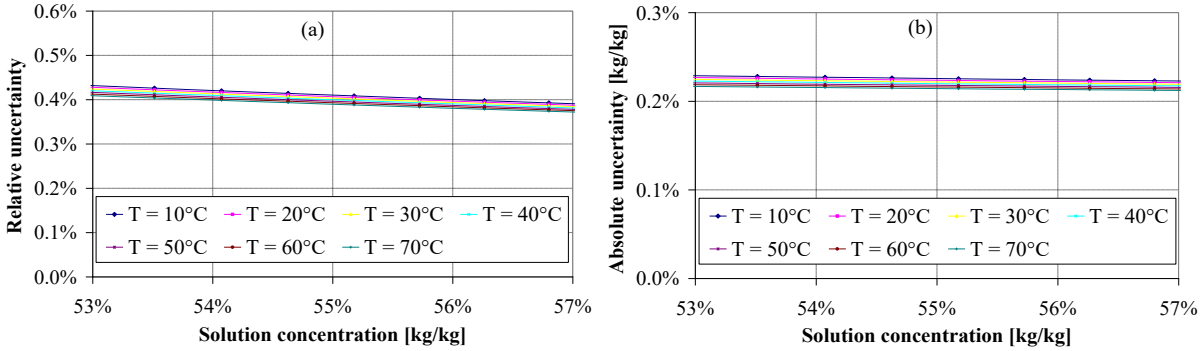

Fig. B.1. Relative (a) and absolute (b) uncertainties of the solution concentration.

B2. Power exchanged in the desorber/condenser calculated based on the HTF temperature change

The power exchanged in the desorber is:

$$Q_2 = m_g \cdot Cp_g \cdot (T_{gi} - T_{go}) \quad (8)$$

The HTF heat capacity Cp_g change is insignificant between the desorber inlet and outlet temperature (temperature change less than 2.5°C in the presented desorption); it is assumed that its uncertainty is approximately zero.

Then, the uncertainty of the power calculation can be expressed as follows:

$$\Delta Q_2 = Cp_g \cdot \sqrt{\left((T_{gi} - T_{go}) \cdot \Delta m\right)^2 + \left(m_g \cdot \sqrt{2 \cdot \Delta T^2}\right)^2} \quad (B.2)$$

$$\Delta Q_2 = m_g \cdot Cp_g \cdot \sqrt{\left((T_{gi} - T_{go}) \cdot \frac{\Delta m}{m}\right)^2 + 2 \cdot \Delta T^2} \quad (B.3)$$

The maximum measured temperature difference T_{go} - T_{gi} during the presented desorption is 2.5 °C. Therefore:

$\Delta Q_2 = 0.2 \cdot 4.2 \cdot \sqrt{(2.5 \cdot 0.1\%)^2 + 2 \cdot 0.2^2} = 0.24\ kW$	

The uncertainty of the condenser power Q_3 measurement is the half of the above since the heat transfer fluid flow rate is divided by two. So:

$\Delta Q_3 = 0.12\ kW$

B3. Power exchanged in the desorber calculated based on solution enthalpy change

The power exchanged in the desorber is:

$$Q_2' = m_{2o} \cdot h_{2o} + m_{vap} \cdot h_{vap} - m_{2i} \cdot h_{2i} \quad (10)$$

Using Eq. (11), Eq. (10) is re-written as follows:

$$Q_2' = m_{2i} \cdot \left[\frac{x_{2i}}{x_{2o}} \cdot h_{2o} + \left(1 - \frac{x_{2i}}{x_{2o}}\right) \cdot h_{vap} - h_{2i}\right] \quad (B.4)$$

The uncertainty $\Delta Q_2'$ can be expressed as follows:

$$\Delta Q_2' = \left[\left(\frac{\partial Q_2'}{\partial x_{2i}} \cdot \Delta x_{2i}\right)^2 + \left(\frac{\partial Q_2'}{\partial x_{2o}} \cdot \Delta x_{2o}\right)^2 + \left(\frac{\partial Q_2'}{\partial h_{2i}} \cdot \Delta h_{2i}\right)^2 + \left(\frac{\partial Q_2'}{\partial h_{2i}} \cdot \Delta h_{2o}\right)^2 + \left(\frac{\partial Q_2'}{\partial h_{vap}} \cdot \Delta h_{vap}\right)^2\right]^{0.5} \quad (B.5)$$

For each measurement point, Eq. (B.x) is applied. The uncertainty have been evaluated in the same way as described in Appendix B.1. For the enthalpy values, only the uncertainties on the temperature and concentration measurements have been taken into account.

B4. Mass of desorbed/absorbed water

The level of the water in the water storage tank is measured with a liquid level (Table A.1). The mass change during a test and its uncertainty can then be calculated as follows:

$$M = \rho \cdot \frac{\pi}{4} \cdot D^2 \cdot h \quad (B.6)$$

$$\frac{\Delta M}{M} = \sqrt{\left(\frac{\Delta \rho}{\rho}\right)^2 + \left(2 \cdot \frac{\Delta D}{D}\right)^2 + \left(\frac{\Delta h}{h}\right)^2} \quad (B.7)$$

ρ: saturated liquid water density. 1000 kg·m^{-3} is assigned to ρ. To estimate the uncertainty Δρ, the maximum deviation between 1000 kg·m^{-3} and the values tabulated in the IAPWS 95 (Wagner et al., 2002, p.186), for temperature between 10 and 16°C (temperature range measured in the tank). Then, Δρ/ρ = 0.1%

D = 0.40 m: diameter of the water storage tank. The uncertainty can be estimated to be ΔD = 0.004 m. So, ΔD/D = 1%.

h: liquid level change in the water storage tank during the test (from the beginning to the end of each test). The uncertainty of the liquid level meter is ± 2 mm (Table A.1). The uncertainty of h is then $\Delta h = \pm 2 \cdot \sqrt{2} \approx \pm 3\, mm$. The average measured level change during the charging tests is 24 mm (3 kg of water). So, the uncertainty in that case would be $\Delta h/h_{min} = 12\%$.

Finally, the uncertainties of the water density ($\Delta\rho/\rho = 0.1\%$) and of the tank diameter ($\Delta D/D = 1\%$) can be neglected and the overall uncertainty be reduced to the uncertainty of the liquid level change. Then, the absolute uncertainty of the mass of desorbed water can be estimated as follows:

$$\Delta M \approx \rho \cdot \frac{\pi}{4} \cdot D^2 \cdot \Delta h = 1000 \cdot \frac{\pi}{4} \cdot 0.4^2 \cdot 0.003 = 0.4\, kg$$

This uncertainty is also high. Actually, different approaches have been used to control the calculated values based on the data from the level meter. These approaches consist of the integration of the mass flow rate measured by the flowmeters at the inlet and outlet of each storage tank:

- by calculating the difference (in volume) between the water storage tank outlet and inlet water: it equals to the difference between the cumulative volumetric flow measured by the volume flowmeters at the tank outlet and inlet:

$$M' = \rho \cdot \underbrace{\int_{t_{start}}^{t_{end}} v_{3o} \cdot dt}_{\substack{\text{Cumulative volumetric flow} \\ \text{at the water storage tank outlet}}} - \rho \cdot \underbrace{\int_{t_{start}}^{t_{end}} v_{3i} \cdot dt}_{\substack{\text{Cumulative volumetric flow} \\ \text{at the water storage tank intlet}}} \approx \rho \cdot \sum_{t_{start}}^{t_{end}} \left(v_{3o} - v_{3i}\right) \cdot \Delta t \qquad \text{(B.8)}$$

- by calculating the difference (in mass) between the solution storage tank outlet and inlet solution: it equals to the difference between the cumulative mass flow measured by the mass flowmeters at the tank outlet and inlet:

$$M'' = \underbrace{\int_{t_{start}}^{t_{end}} m_{2i} \cdot dt}_{\substack{\text{Cumulative mass flow at the} \\ \text{solution storage tank inlet}}} - \underbrace{\int_{t_{start}}^{t_{end}} m_{2o} \cdot dt}_{\substack{\text{Cumulative mass flow at the} \\ \text{solution storage tank oulet}}} \approx \sum_{t_{start}}^{t_{end}} \left(m_{2i} - m_{2o}\right) \cdot \Delta t \qquad \text{(B.9)}$$

Δt = 5 s (data are recorded every 5 seconds).

The agreements between M, M' and M'' is in the range of 0.3 kg.

References

Bales, C., 2008. Final report of Subtask B "Chemical and Sorption Storage" The overview.

Bales, C., Nordlander, S., 2005. TCA Evaluation - Lab Measurements, Modelling and System Simulations (No. ISRN DU-SERC--91--SE). Högskolan Dalarna, Borlänge.

Berthemot, 1830a. Mémoire pour servir à l'histoire des bromures. Gay-Lussac, Arago (editors). Annales de chimie et de physique 44.

Berthemot, 1830b. Mémoire pour servir à l'histoire des bromures métalliques. Journal de chimie médicale, de pharmacie et de toxicology Tome VI.

Berthiaud, J., Mazet, N., Luo, L., Stitou, D., Descamps, I., 2006. Long-distance transport of thermal energy using sorption cycles. Presented at the ATI Conference.

Boryta, D.A., 1970. Solubility of lithium bromide in water between -50.deg. and +100.deg. (45 to 70% lithium bromide). Journal of Chemical & Engineering Data 15, 142–144.

Dean, J.A., 1999. Solubility of Inorganic compounds ans Metals Salts of Organic Acids in Water at Various Temperatures. Lange's Handbook of Chemistry (Table 5.2, page 5.15), 15th ed. McGraw-Hill, New York.

Duvall, K.N., Dirksen, J.A., Ring, T.A., 2001. Ostwald-Meyers metastable region in LiBr crystallization-comparison of measurements with predictions. Journal of Colloid and Interface Science 239, 391–398.

Figliola, R.S., 2010. Theory and Design for Mechanical Measurements, 5th ed. John Wiley & Sons, Inc.

Florides, G.A., Kalogirou, S.A., Tassou, S.A., Wrobel, L.C., 2003. Design and construction of a LiBr-water absorption machine. Energy Conversion and Management 44, 2483–2508.

Fujita, T., 1993. Falling liquid films in absorption machines. International Journal of Refrigeration 16, 282–294.

Haar, L., Gallagher, J.S., Kell, G.S., 1984. NBS/NRC steam tables: thermodynamic and transport properties and computer programs for vapor and liquid states of water in SI units, Hemisphere Publishing Corp., New York.

Hauer, A., 2010. Compact thermal storages: potentials and limitations for different applications. Presented at the EUROSUN 2010, 2nd International Conference on Solar Heating, Cooling and Buildings.

Hellmann, H.-M., Grossman, G., 1996. Improved property data correlations of absorption fluids for computer simulation of heat pump cycles. ASHRAE Transactions 102, 980–997.

Herold, K.E., Radermacher, R., Klein, S.A., 1996. Absorption Chillers and Heat Pumps. CRC Press Inc, Boca Raton.

Hihara, E., Saito, T., 1993. Effect of surfactant on falling film absorption. International Journal of Refrigeration 16, 339–346.

Jones H.C., Strong W.W., 1910. A study of the absorption spectra of solutions of certain salts of potassium, cobalt, nickel, copper, chromium, erbium, praseodymium, neodymium, and uranium as affected by chemical agents and by temperature. Washington D.C.: Carnegie Institution of Washington.

Kato, Y., 2010. Feasibility of vehicle thermal energy storage (VTES). Presented at the 12th International Conference on Energy Storage (Innostock 2012).

Kerskes, H., Mette, B., Bertsch, F., Asenbeck, S., Drück, H., 2012. Chemical energy storage using reversible solid/gas-reactions (CWS) – results of the research project. Energy Procedia 30, 294–304.

Kessis, J.J., 1965. The water-lithium bromide systems. Bulletin de la Societe Chimique de France 1, 48–52.

Lass-Seyoum, A., Blicker, M., Borozdenko, D., Friedrich, T., Langhof, T., 2012. Transfer of laboratory results on closed sorption thermo- chemical energy storage to a large-scale technical system. Energy Procedia 30, 310–320.

Le Pierrès, N., Liu, H., Luo, L., 2011. $CaCl_2/H_2O$ absorption seasonal storage of solar heat. Presented at the International Conference for Sustainable Energy Storage.

Lee, R.J., DiGuilio, R.M., Jeter, S.M., Teja, A.S., 1990. Properties of lithium bromide-water solutions at high temperatures and concentrations. II. Density and viscosity. ASHRAE Transactions 96, 709–714.

Linke, W.F., Seidell, A., 1965. Solubilities of Inorganic and Metal Organic Compounds, Vol. II, 4th. ed. American Chemical Society, Washington D. C.

Liu, H., N'Tsoukpoe, K.E., Le Pierrès, N., Luo, L., 2011. Evaluation of a seasonal storage system of solar energy for house heating using different absorption couples. Energy Conversion and Management 52, 2427–2436.

Marias, F., Tanguy, G., Wyttenbach, J., Rouge, S., Papillon, P., 2011. Thermochemical Storage: first results of pilot storage system with moist air. Presented at the ISES World Congress.

Mauran, S., Lahmidi, H., Goetz, V., 2008. Solar heating and cooling by a thermochemical process. First experiments of a prototype storing 60 kWh by a solid/gas reaction. Solar Energy 82, 623–636.

Michel, B., 2012. Procédé thermochimique pour le stockage intersaisonnier de l'énergie solaire : modélisation multi-échelles et expérimentation d'un prototype sous air humide (PhD thesis) [French]. Université de Perpignan Via Domitia.

Moffat, R.J., 1988. Describing the uncertainties in experimental results. Experimental Thermal and Fluid Science 1, 3–17.

Muñoz-Portero, M.J., García-Antón J., Guiñón J.L., Pérez-Herranz V., 2006. Corrosion of copper in aqueous lithium bromide concentrated solutions by immersion testing. Corrosion 62, 1018–1027.

N'Tsoukpoe, K.E., Liu, H., Le Pierrès, N., Luo, L., 2009. A review on long-term sorption solar energy storage. Renewable and Sustainable Energy Reviews 13, 2385–2396.

N'Tsoukpoe, K.E., Le Pierrès, N., Luo, L., 2012a. Numerical dynamic simulation and analysis of a lithium bromide/water long-term solar heat storage system. Energy 37, 346–358.

N'Tsoukpoe, K.E., Le Pierrès, N., Luo, L., 2012b. Experimentation of a LiBr-H_2O absorption process for long term solar thermal storage. Energy Procedia 30, 331-341.

N'Tsoukpoe, K.E., Le Pierrès, N., Luo, L., 2013. Experimentation of a LiBr−H_2O absorption process for long term solar thermal storage: prototype design and first results. Energy 53, 179−198.

Nývlt, J., 1977. Solid-liquid phase equilibria. Elsevier Scientific Pub.

Quinnell, J.A., Davidson, J.H., 2012. Mass transfer during sensible charging of a hybrid absorption/sensible storage tank. Energy Procedia 30, 353–361.

Saul, A., Wagner, W., 1987. International equations for the saturation properties of ordinary water substance. Journal of Physical and Chemical Reference Data 16, 893–901.

Schaube, F., Kohzer, A., Schütz, J., Wörner, A., Müller-Steinhagen, H., 2012. De- and rehydration of $Ca(OH)_2$ in a reactor with direct heat transfer for thermo-chemical heat storage. Part A: Experimental results. Chemical Engineering Research and Design. (in press, DOI: 0.1016/j.cherd.2012.09.020)

Schmidt, T., Rammelberg, H.U., Rönnebeck, T., N'Tsoukpoe, K.E., Fopah Lele, A., Belz, K., Rohde, C., Köllner, J.K., Korhammer, K., Opel, O., Ruck, W.K.L., 2012. Conception of a heat storage system for household applications. Presented at the "7th International Renewable Energy Storage Conference and Exhibition" (IRES 2012), Berlin, Germany.

Shkatulov, A., Ryu, J., Kato, Y., Aristov, Y., 2012. Composite material "$Mg(OH)_2$/vermiculite": A promising new candidate for storage of middle temperature heat. Energy 44, 1028–1034.

Tanguy, G., Marias, F., Rouge, S., Wyttenbach, J., Papillon, P., 2012. Parametric studies of thermochemical processes for seasonal storage. Energy Procedia 30, 388–394.

Tatsidjodoung, P., Le Pierrès, N., Luo, L., 2013. A review of potential materials for thermal energy storage in building applications. Renewable and Sustainable Energy Reviews 18, 327–349.

Van Helden, W.G., 2009. Interview with Wim van Helden, Operating Agent of IEA SHC/ECES Task42/24 for the Solar Heating and Cooling program, at ESTEC 2009. http://www.youtube.com/watch?v=7tjJ7baKQVE&noredirect=1 accessed on 1st March 2013.

Ventas, R., Lecuona, A., Legrand, M., Rodríguez-Hidalgo, M.C., 2010. On the recirculation of ammonia-lithium nitrate in adiabatic absorbers for chillers. Applied Thermal Engineering 30, 2770–2777.

Wagner W., Pruß A., 2002. The IAPWS formulation 1995 for the thermodynamic properties of ordinary water substance for general and scientific use. Journal of Physical and Chemical Reference Data 31:387–535

Weber, R., 2010. Long-term heat storage with NaOH. Presented at the EUROSUN 2010, 2nd International Conference on Solar Heating, Cooling and Buildings.

Zondag, A., Kalbasenka, A., Van Essen, M., 2010a. An evaluation of the economical feasibility of seasonal sorption heat storage. Presented at the 5th International Renewable Energy Storage Conference IRES 2010.

Zondag, A., Kikkert, B.W., Smeding, S., Boer, R.D., Bakker, M., 2012. Prototype thermochemical heat storage with open reactor system. Presented at the 12th International Conference on Energy Storage (Innostock 2012).